Anharmonic Effects on the Dynamics of Solid Aluminium from *Ab-Initio* Simulations

Donat J. Adams

*University of Bern, CH-3012 Bern, Switzerland**

Lin Wang and Gerd Steinle-Neumann

Bayerisches Geoinstitut, Universität Bayreuth, D-95440 Bayreuth, Germany

Daniele Passerone

Empa – Swiss Federal Laboratories for Materials Science and Technology, CH-8600 Dübendorf, Switzerland

Sergey V. Churakov

University of Bern, CH-3012 Bern, Switzerland; Laboratory for Waste Management, Paul Scherrer Institute, CH-5232 Villigen-PSI, Switzerland

(Dated: October 26, 2020)

Abstract

Two approaches to simulations of phonon properties of solids beyond the harmonic approximation, the Self-Consistent *ab-initio* Lattice Dynamics (SCAILD) and Decoupled Anharmonic Mode Approximation (DAMA) are critically benchmarked against each other and molecular dynamics simulations using a density-functional-theory description of electronic states, and compared to experimental data for *fcc aluminium. The temperature-dependence of phonon dispersion and the phonon density-of-states, heat capacity, and the mean atomic displacement for fcc aluminium are examined with these approaches at ambient pressure. A comparison of results obtained with the harmonic approximation to the ones predicted by SCAILD and DAMA reveal a negligible anharmonic contribution to phonon frequencies, a small, but significant influence on heat capacity, and a strong effect on atomic mean-square displacement. The phase space accessed with SCAILD and DAMA is reduced relative to molecular and harmonic lattice dynamics simulations. In particular the DAMA results are in good agreement with displacement amplitudes determined by the Debye-Waller factor in X-ray diffraction experiments.*

I. INTRODUCTION

Electronic and structural properties of metallic aluminium are well reproduced by Kohn-Sham (KS) density-functional-theory (DFT) [e.g., 1–3], because of a small number of valence electrons and free-electron like properties of electronic states with low dispersion. Aluminium has thus served as a reference system for the development and testing of new theoretical and computational approaches [e.g., 4, 5]. At ambient conditions, aluminium crystallises in the face center cubic (*fcc) structure, in which it is stable up to the melting point (T_M = 933 K) [6]. Physical properties of aluminium are well known experimentally over a wide temperature (T) range, including phonon dispersion curves [e.g., 7] and density-of-states, the latter available up to 800 K [8]. Also, the Debye-Waller (DW) factor has been measured by X-ray diffraction up to T_M [9] which provides access to the atomic dynamics in the system, as electron-electron and electron-phonon contributions to the DW factor are expected to be negligible for aluminium, documented by the Debye-like behaviour of electronic conductivity well beyond the T-range considered here [e.g., 3, 10]. Combined, high-quality T-dependent*

* donat.adams@geo.unibe.ch

phonon data and mean atomic displacements for aluminium provide a well defined system for testing the performance of computational methods for simulations of metallic solids and the quantification of anharmonic effects in particular.

Thermodynamic and thermo-elastic properties of crystalline materials have usually been modeled at the DFT level either by using the molecular dynamics (MD) or the harmonic lattice dynamics (h-LD) approach. In MD, atoms in a supercell are propagated as classical particles according to the Hellmann-Feynman forces acting on them [11], and the ensemble average of physical properties is obtained by averaging a time series of atomic configurations based on the ergodic theorem [12]. As a consequence, MD simulations fail to describe low-T properties of materials, i.e., below the Debye temperature ($\Theta_D = 428$ K for Al [13]), where quantum effects matter. By contrast, h-LD computes effective phonon frequencies ω for the eigenmodes which are T-independent and populated according to Bose-Einstein statistics, taking the quantum-nature of lattice vibrations into account. This approach is implemented either in linear response theory [14] or the finite displacement method, e.g., the PHON [15] or PH [14] codes. The LD approach is appealing for a number of reasons:

i. *Phonon frequencies can be directly compared to measurements.*

ii. *By integrating the phonon density-of-states, or directly computing the partition sum, one has direct access to the vibrational contribution to Helmholtz energy (A_{vib}), while the computation of energies from MD simulations requires thermodynamic integration [e.g., 1, 16, 17].*

iii. *Simulations of thermodynamic properties by LD require significantly less computational resources as fewer configurations are evaluated compared to MD.*

The major drawback of h-LD is the fact that it does not account for T-dependence of lattice vibrations and fails completely when the potential energy surface shows negative curvature. To address this shortcoming, a number of strategies have been pursued to generalise the LD method for applications in which anharmonicity contributes significantly to the vibrational behaviour. The available methods range from using anharmonic force constants derived from multiple displacement amplitudes, as implemented in the ALAMODE *code [18], to iteratively optimizing A_{vib} in an inherently harmonic potential and computing an*

atomic probability distribution, the Stochastic Self-Consistent Harmonic Approximation (SSCHA) *[19]. Within generalised LD approaches, the* Self-Consistent *ab-initio* Lattice Dynamics (SCAILD) *method [20] and the* Decoupled Anharmonic Mode Approximation (DAMA) *[21] can be viewed as two endmembers:*

i. SCAILD self-consistently determines the mean atomic displacement at given T by searching for the repulsive region of the potential. In that region the effective force constants are obtained. The harmonic approximation is then applied to calculate the crystallographic eigenmodes; SCAILD thus partly accounts for the anharmonicity of the atomic displacement along the mode-eigenvectors as well as for the coupling of different modes (phonon-phonon interactions).

ii. DAMA stays within the independent phonon approximation by decoupling the vibrational modes using the harmonic mode eigenvectors, but accounts for the full potential along these directions.

In this work, we use DAMA and SCAILD to compute phonon ω and physical properties of solid aluminium at ambient pressure. Results are compared to MD simulations and experimental data. Due to the stability of the fcc structure, anharmonic effects are less pronounced than those typically found in crystals that are dynamically stable only at high T, including the bcc phase of some group-IV metals (titanium, zirconium and hafnium) [22–27]. For aluminium, we explore the influence of anharmonicity on the T-dependent phonon ω, the heat capacity and mean atomic displacement.

II. METHODS

Simulations of aluminium in the fcc structure are performed at $T = 500$ K, 700 K and 900 K, i.e., above Θ_D. Lattice parameters at T are taken from the DAMA results (Figure 1) in all other approaches. The simulation supercells contain 32 cells for PH and DAMA ($4 \times 4 \times 2$), 64 cells for PHON and SCAILD ($4 \times 4 \times 4$) and 256 atoms for MD ($4 \times 4 \times 4$ of the conventional unit cell). SCAILD and DAMA simulations are based on initial guesses of the eigenvectors from h-LD results obtained with PHON [15] and PH [14], respectively. Molecular dynamics simulations are performed in the canonical ensemble, keeping the number of atoms N and the cell volume V fixed; T is controlled by a Nosé thermostat [28, 29]. The

equations of motion are integrated with a time step of 1 fs, and equilibrium trajectories comprise 20 ps.

Energies and Hellmann-Feynman forces are evaluated with KS-DFT based methods. The electronic structure is calculated with a plane-wave basis set, using the Vienna Ab-Initio Simulation Package (VASP) *[30] for the PHON, SCAILD and MD simulations, and* Quantum Espresso *[31] for PH and DAMA. The generalised gradient approximation [32] is used to describe the exchange and correlation potential combined with ultrasoft pseudopotentials [33, 34] for a* $3s^2 3p^1$ *valence electron configuration. Reciprocal space is sampled with the* Γ*-point for MD, and a* $4 \times 4 \times 4$ *Monkhorst-Pack grid for the LD-based methods, respectively. Iterative optimisation is performed to enforce convergence of total energy to* $< 10^{-6}$ *eV/atom and that of the Hellmann-Feynman forces to* $< 10^{-4}$ *eV/Å.*

In SCAILD simulations the eigenvectors obtained with the PHON code provide an initial guess for the collective displacement of the atoms using the SCPH software [20]. These are used to excite all phonon modes that are commensurate with the supercell by varying displacement amplitudes depending on ω *and* T*. Resulting forces are projected onto the polarisation vectors of the phonon modes to determine effective* ω*. This procedure is iterated until all* ω *are converged. Here we use an* ω*-difference of 1 GHz as a convergence criterion, which typically can be achieved within 20 iterations. Tests with smaller (*$3 \times 3 \times 3$*) and larger (*$5 \times 5 \times 5$*) supercells show slight shifts in the phonon dispersion curves, mostly due to different reciprocal space vectors* $\mathbf{q}$ *being commensurate with the cell, but the resulting phonon density-of-states obtained with different supercells are indistinguishable.*

In the DAMA simulations, the total energy is evaluated from configurations with atoms displaced along the eigenvectors of harmonic vibrational modes. The resulting energy curves (vs. atomic displacement) are used to calculate the anharmonic eigenstates. Convergence of low-energy phonon excitations is critical for an accurate determination of A_{vib}*, while numerical errors due to the energy contribution of higher-*ω *states are suppressed in the population statistics. With an energy cutoff of 30 eV for vibrational energies, differences in* ω *in the DAMA simulations are also converged to within 1 GHz.*

For the purpose of this study we have extended the DAMA formalism to reciprocal space sampling ($\mathbf{q}$*-DAMA). The previous implementation was restricted to* Γ*-point sampling [21], and it only permitted the computations of eigenstates at* $\mathbf{q}$*-vectors commensurate with the supercell setup. In* $\mathbf{q}$*-DAMA, a linear-response calculation is performed and the full linear-*

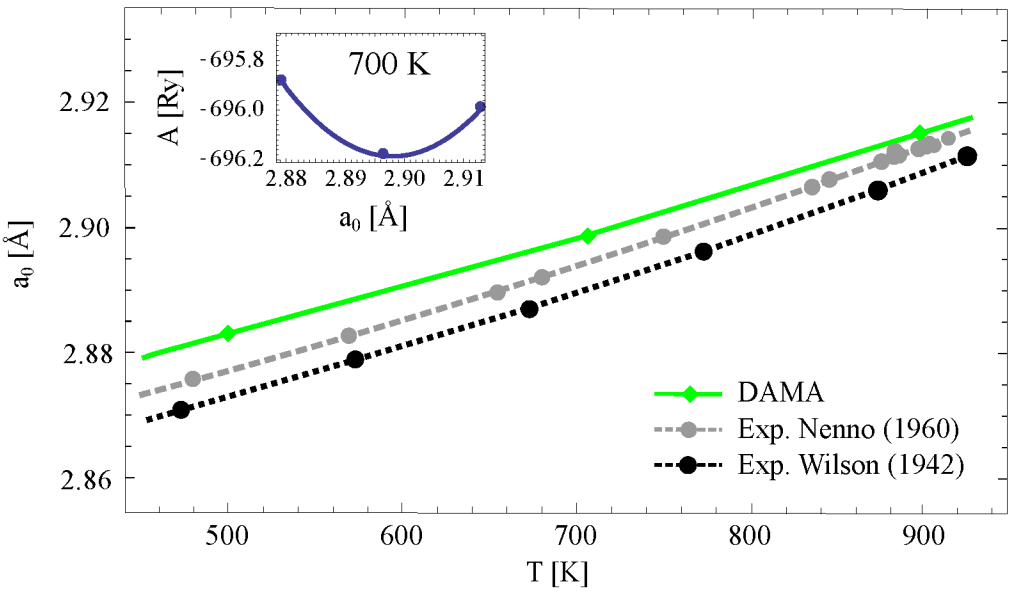

FIG. 1. Temperature dependence of lattice constant for *fcc aluminium. Results from DAMA simulations (blue) at* $T = 500$ *K (2.879 Å),* $T = 700$ *K (2.896 Å) and* $T = 900$ *K (2.913 Å) are compared to experimental data [36] (black) and [37] (grey). Inset: Lattice constant determination at* $T = 700$ *K by Helmholtz energy minimisation from a discrete set of* V *and fit by a second-order polynomial to the results. Results show a marginally lower coefficient of thermal expansion* $\alpha = 25.2 \times 10^{-6}$ K^{-1} *than experiments with* $\alpha = 26.6 \times 10^{-6}$ K^{-1} *[36, 38].*

response Hamiltonian is retained; then a set of $\mathbf{q}$*-points and calculated harmonic polarisation vectors* $\epsilon^{sx}(\mathbf{q})$ *(for atom number* s *and coordinates* x*) are transferred to a supercell commensurate with the* $\mathbf{q}$*-point grid. In this cell, vibrational modes along the polarisation vectors* $\epsilon^{sx}(\mathbf{q})$ *are computed using the full Hamiltonian. Following the same approach as in harmonic theory [15, 35], the phonon dispersion is interpolated between the discrete set of* $\mathbf{q}$*-vectors at which they are evaluated explicitly.*

The influence of anharmonic effects is evaluated comparing phonon properties computed with SCAILD and DAMA to the results of the underlying harmonic approximation (i.e., PHON and PH, respectively).

III. RESULTS AND DISCUSSION

A. Phonons

Phonon dispersion curves computed by h-LD using the PHON and PH codes closely reproduce previously computed dispersion curves [39] for fcc aluminium and low T data (80 K) from neutron diffraction experiments [7] (Figure 1 in the supplemental material). Small differences in ω between PHON or PH arise from the implementations of the small displacement method and the numerical strategy for diagonalization in the respective codes, as well as the underlying electronic structure computations and the slightly different pseudopotentials used. The overall agreement of computed ω in both sets of simulations with low T neutron diffraction data shows the robustness of h-LD for phonon calculations in Al.

Increasing T with associated lattice expansion lead to a shift of ω to lower values due to a decrease in strength of interatomic interactions (Figure 2; Figure 2 of the supplemental material for a comparision of the phonon-density-of-states each method with experiment). For the PHON simulations, the density-of-states (evaluated with a smearing of 0.5 THz) shows a bimodal distribution with maxima in the range between 4.0-4.5 THz and around 8.0 THz. With increasing V (or equivalently T), they shift to slightly lower ω (Figure 2 in the online supporting material).

The maximum above 4.0 THz reflects T-averaged maxima in ω for the transverse acoustic (TA) modes at high symmetry points at the Brillouin zone boundary, X (0, 1/2, 0), L (1/2, 1/2, 1/2) and K (3/8, 3/8, 3/4), as well as a nearly dispersionless branch along X-K. The maximum near 8.0 THz represents the longitudinal acoustic (LA) branch at X and L, with some contribution from the maximum along the K-Γ direction, consistent with the analysis of experiments [e.g., 40]. The phonon density-of-states are qualitatively consistent with the neutron diffraction data [8], although the neutron experiments show the maximum representing the TA modes just below 5 THz both at $T = 525$ K and $T = 775$ K (Figure 2).

At 500 K, phonon dispersion curves and especially phonon density-of-states (Figure 2) of the harmonic approximation, SCAILD and DAMA differ only slightly, which indicates that thermal excitations and atomic displacement amplitudes are small and thus anharmonic effects are negligible (Section III C). If we compare the phonon density-of-states between PH and SCAILD at $T = 900$ K (Figure 2 d-f), the blue-shift of modes due to smaller

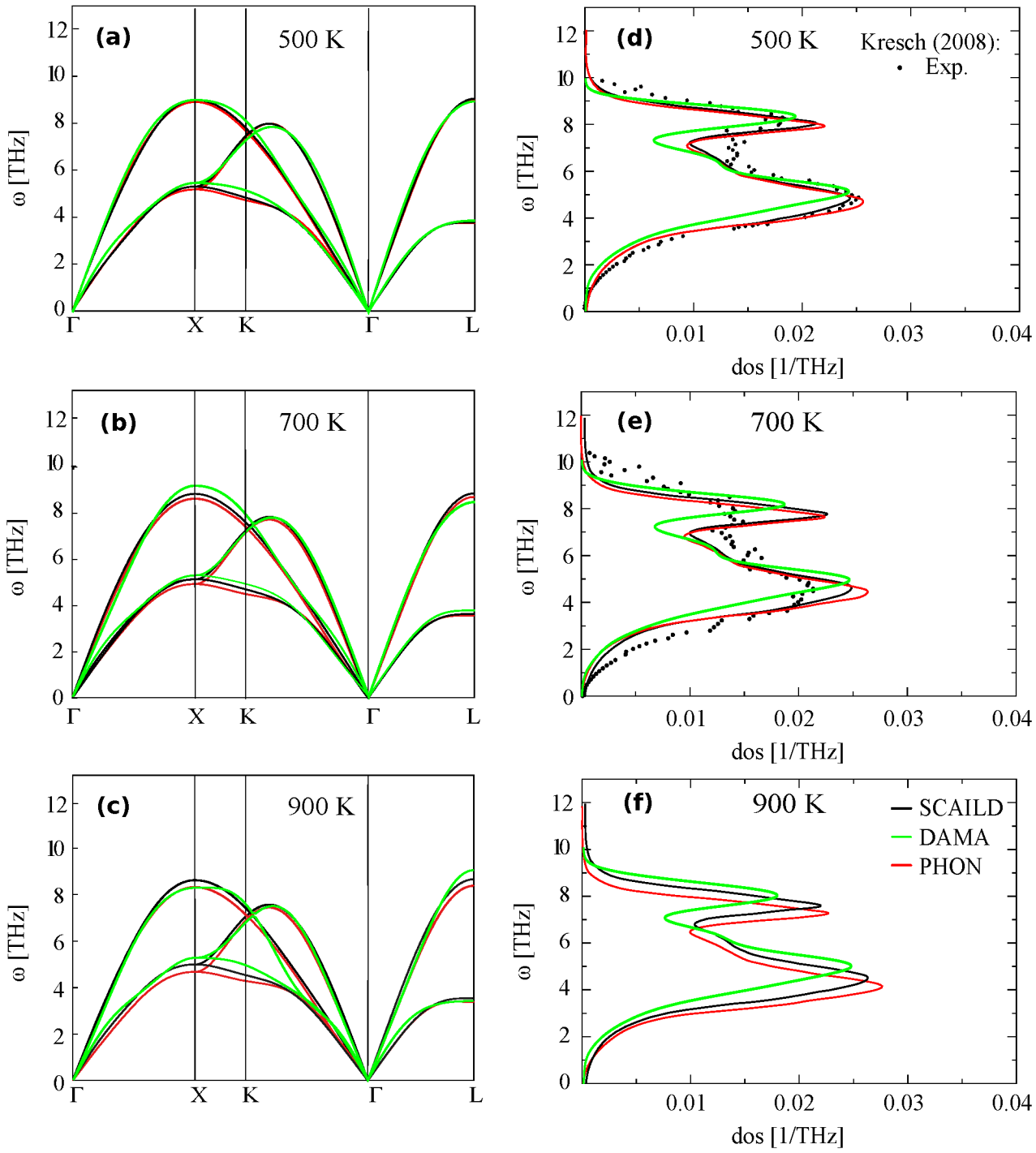

FIG. 2. Phonon properties of *fcc aluminium at (a+d) 500 K (lattice parameter 2.879 Å), (b+e) 700 K (2.896 Å) and (c+f) 900 K (2.913 Å). Phonon dispersion curves (a-c) show results of the harmonic (PHON, red), SCAILD (black) and DAMA (green) simulations. The phonon density-of-states (d-f) are compared to experimental data by Kresch* et al. *[8] at 525 K (d) and 775 K (e).*

atomic displacement in SCAILD becomes significant. This blue-shift is small not only for $T = 500$ K, but also for 700 K, where thermal excitations and therefore vibrational amplitudes are reduced. A subtle increase in the phonon density-of-states at intermediate ω – shifting from 6.2 THz ($T = 500$ K) to 6.6 THz ($T = 900$ K) – is visible in all simulations and the neutron experiments at $T = 525$ K; its origin can not directly be deduced from dispersion curves along the high symmetry directions in the Brillouin zone, but is also visible in the experiments at 80 K [40].

The shape of the phonon density-of-states and maxima at $T = 500$ K from neutron experiments [8] are better reproduced by the DAMA than the PHON or SCAILD simulations (Figure 2). However, in the experiments maxima are less pronounced and broader, and a significant contribution persists to larger ω. These features suggest that in the experiments higher-order contributions are not completely filtered out. This could also cause the scattering visible in the experimental data.

The changes of mode frequencies with V can be quantified with the mode Grüneisen parameter $\gamma_{\mathbf{q},\nu} = -\partial\left(\ln\omega\left(\mathbf{q},\nu\right)\right)/\left(\partial \ln V\right)$, in which the frequency ω for mode ν is evaluated. These values are reported in Table I at the high-symmetry boundary points of the Brillouin zone, X and L (Figure 2). The LA mode shows a significantly larger γ than the TA mode. Differences in γ between the PHON and PH results reflect the variability of ω in the harmonic approximation already discussed. Positive values of γ indicate a red-shift of phonon modes (decreasing ω), directly visible in the phonon dispersion curves (Figure 2; Figure 1 in the supplemental material).

	X point		L point	
	LA mode	TA mode	LA mode	TA mode
PHON	1.92	2.90	2.03	2.88
PH and DAMA	1.87	2.45	1.95	2.61
SCAILD	1.19	1.68	1.18	1.78

TABLE I. Mode Grüneisen parameters for the longitudinal and transverse modes at the X and L high symmetry points on the Brillouin zone boundary. As the TA modes are degenerate on the zone boundary, only one value is reported.

Phonon-phonon interactions, as accounted for in the SCAILD approach, slightly coun-

teract the decrease in ω in response to the shallower potential well due to the V-increase, and lead to slightly larger ω relative to the h-LD results (Figure 2). The blue-shift of the SCAILD results compared to those from PHON increases with T, leading to smaller values of γ at the Brillouin zone boundary by a factor of ~ 0.6. This shift of phonon ω and the increased dispersion (reduced maximum) is reflected in the phonon density-of-states, most prominently for the TA peak in the ω-range of $4.0-4.5$ THz. Larger ω in the SCAILD simulations compared to PHON can be expected, as the effective curvature and associated atomic displacement (Section III C) are determined iteratively. At larger displacements, the interaction between atomic cores adds repulsion to the potential, leading to increased curvature, and therefore ω.

Contrary to SCAILD and the harmonic approach, where excitation energies (E_ν for a specific mode) are equally spaced and all transitions appear at the same ω, anharmonicity in the DAMA approach leads to an increase in higher excitation energies [21] which results in a finite ω-range of transitions: There is a sharp onset that corresponds to the fundamental excitation and a distribution at higher ω which we illustrate for the TA frequency at the L-point (Figure 3). This effect can be large for strongly anharmonic systems like Na_3AlF_6 cryolite [21], but for aluminium it is insignificant. Even at 900 K – where it is largest – the ω-shift in response to T following the Boltzmann distribution for occupation is negligibly small and does not exceed a few 10 GHz.

B. Heat capacity

In computing the Helmholtz energy A_{vib} from the partition sum of the excitation spectrum, the increase for higher E_ν in DAMA has a stronger influence. We explore this effect by computing the heat capacity from the three LD-based approaches at T of our simulations. As we consider equilibrium volumes only ($P = 0$), isochoric and isobaric heat capacities are the same, with $c_{P,\mathrm{vib}} = -T\left(\partial^2 G_{\mathrm{vib}}/\partial T^2\right)_P = -T\left(\partial^2 A_{\mathrm{vib}}/\partial T^2\right)_V$. In order to compare to experimental data [41] we add the electronic contribution $c_{P,\mathrm{el}}$ to $c_{P,\mathrm{vib}}$ (Figure 4). At 500 K, differences between the approaches are negligible, and we obtain results that are in good agreement with both prior computations [39] and experiments. For higher T, the PHON and DAMA results closely follow those of Grabowski et al. *[39], but start to deviate from the experimental measurements due to multi-phonon processes that play a significant role*

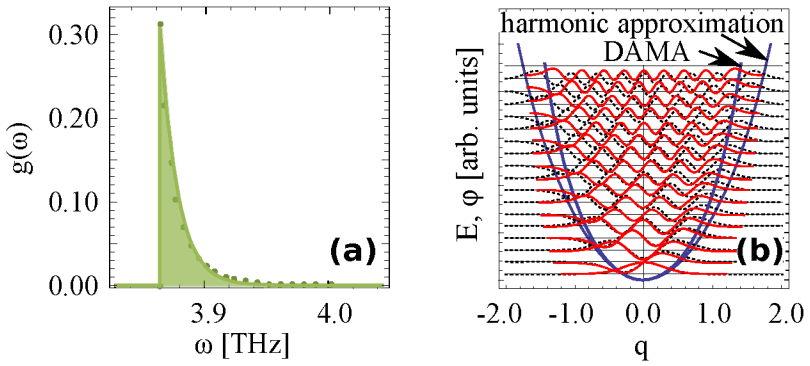

FIG. 3. a) Peak broadening from DAMA calculations affecting the vibrational density-of-states associated with the transverse mode at the L-point with $\omega = 3.87$ THz for the 500 K simulation. b) Sketch illustrating the full potential (DAMA) and its harmonic approximation as well as the larger extent of the vibrational wave function within harmonic theory (dashed black) compared to DAMA (red). The wave functions $\varphi(q)$ are plotted at energy levels E corresponding to different ω.

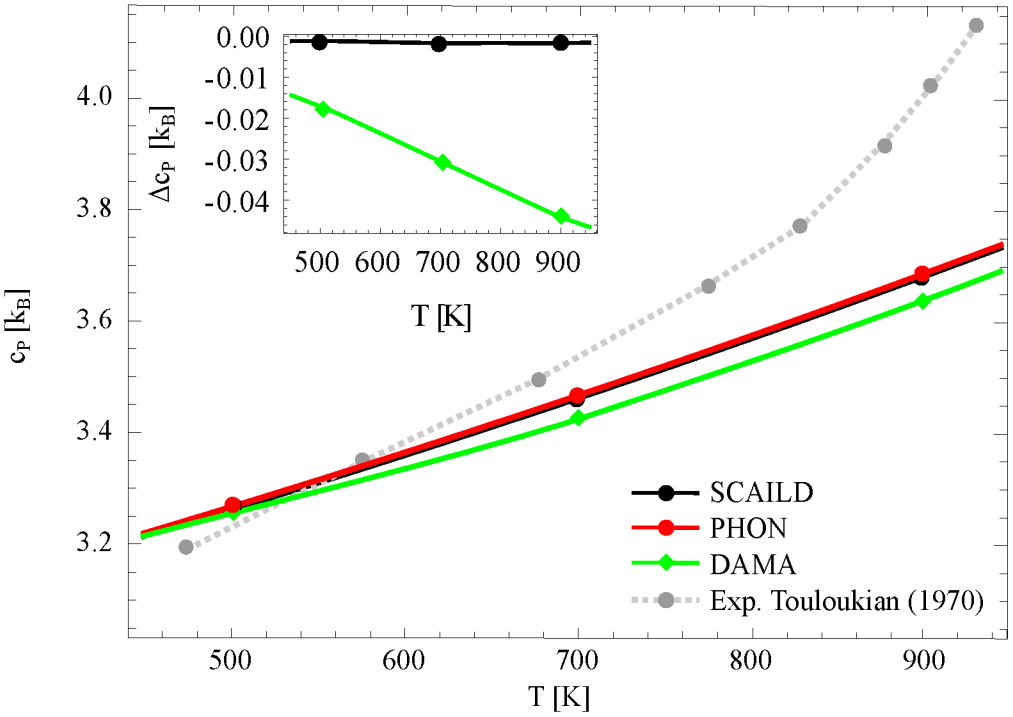

FIG. 4. Heat capacity at constant pressure for *fcc aluminium in units of the Boltzmann constant* k_B. *Experimental data [41] (grey) are compared to results from simulations with SCAILD (black), h-LD (PHON, red) and DAMA (green). Inset: Heat capacity difference* Δc_p *calculated from* $c_{p,\mathrm{SCAILD}} - c_{p,\mathrm{PHON}}$ *(black) and* $c_{p,\mathrm{DAMA}} - c_{p,\mathrm{PHON}}$ *(green), respectively.*

as the solid approaches melting. The DAMA results are lower in c_P, e.g., by 0.03 k_B at 700 K, reflecting the steeper potential (Figure 3) and the resulting non-equidistant excitation spectrum. In the phonon dispersion curves these deviations between qh-LD and SCAILD, on the one hand, and DAMA, on the other hand, are not evident because only the lowest excitation is considered in the latter.

While at first glance this effect appears to lead to a worse agreement with the experimental measurements (Figure 4), multi-phonon contributions at high T will result in an increase in c_P. Katsnelson et al. *[42] explored three- and four-phonon processes for fcc potassium, as an alkaline also a simple metal, and find a contribution of ~ 0.13 k_B at $T/T_m = 0.75$ (corresponding to 700 K in Al) to c_V. Tentatively adding this to the DAMA results at 700 K, total c_P reaches a value of 3.54 k_B, in good agreement with the experimental measurements, with 3.50 k_B at 676 K [41]. At 900 K, just below T_M of Al, such a consideration is no longer meaningful.*

C. Structure and Atomic Dynamics

In a solid, atoms vibrate about their equilibrium position, the amplitude of which can be measured by the Debye-Waller factor in X-ray diffraction experiments [9] in the absence of strong electron-phonon coupling. The displacement amplitudes in the different computational approaches serve as an independent measure to assess the applicability of the SCAILD and DAMA approximations for aluminium, complementarily to ω-based properties. In MD simulations, the mean square displacement (MSD) can be calculated directly, and we find the MSD to reach a stable plateau after the velocity auto-correlation has decayed to zero (~ 100 fs), with values significantly larger than the experimentally determined amplitudes (Figure 5). A similar discrepancy has been reported for the MSD in vitrious SiO_2, where experiments find a MSD of 0.0285(8) Å^2 at room T [43], while ab-initio MD simulation [44] predict values of ~ 0.05 Å^2 for Si and ~ 0.08 Å^2 for O. In this context it is worth pointing out that the equilibrium structure in the MD simulations in terms of the radial distribution function (RDF) (Figure 6) appears to differ from the input structure and the experimental lattice, with distances to the nearest (and higher) neighbour shells determined from the peak (mode of the distribution) of the RDF shifted to smaller values by $0.05 - 0.10$ Å, and skewed to larger distances in MD for the first coordination shell. The mean of the distribution,

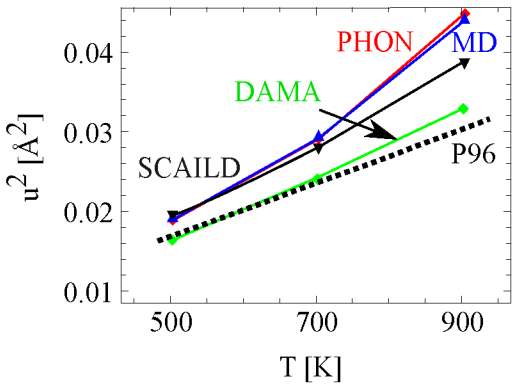

FIG. 5. Atomic mean square displacement in *fcc aluminium inferred from the experimentally measured Debye-Waller factor (P96) [9], DAMA (green diamonds), SCAILD (black triangles down), PHON (red quares) and MD calculations (blue triangles up).*

determined up to the first minimum in the RDF remains at the same distance, reiterating that the mean is more appropriate in describing interatomic distances than the mode [45].

For the LD-based approaches, averaging is performed over vibrational eigenstates: For each polarisation vector the mean value of the amplitude can be calculated, and individual contributions to displacement can be summed up through the variance matrix: The eigenvectors of the variance matrix correspond to the main axes of the vibrational ellipsoid which is a sphere for the cubic system considered here [21]. Mean square displacements from the MD, PHON and the SCAILD are similar at 500 K (Figure 5); with increasing T, MD and PHON values remain close to one another, i.e., significantly larger than inferred from the DW factor. Approximating anharmonicity and many-body interactions in calculating vibrational ω, SCAILD yields notably lower values for the MSD compared to MD and PHON. Considering anharmonicity for vibrational ω and the phonon wave functions in an independent mode approximation, DAMA simulations lead to MSD values that are in good agreement with the DW factors for all T. This suggests that for aluminium the approximation to many-body interactions provided by SCAILD is insignificant, and that the anharmonic potential (DAMA) sufficiently describes the underlying atomic dynamics.

Both SCAILD and DAMA simulations rely on the underlying lattice for the determination of vibrational amplitudes, and consequently their RDF maxima are centered at the equilibrium positions (Figure 6). The distribution of distances in both approaches is symmetric around

the equilibrium position, which is a consequence of the underlying harmonic potential in SCAILD; a narrower potential shape in DAMA and in turn stronger localised wave functions (Figure 3) result in a slightly narrower distribution.

The displacements that we find with both the SCAILD, but particularly the DAMA simulations, suggest that investigations of electron-phonon coupling that are based on the frozen-phonon approach may be biased towards too large displacements [e.g., 46, 47]. Similarly, electrical conductivity estimates of solid metals using a Kubo-Greenwood approach [e.g., 48–50] may suffer from too large changes in electronic band structure from the MD configurations they are based on.

IV. CONCLUSIONS

We have benchmarked three different approaches based on Hellmann-Feynman forces from DFT-based methods to compute the high-T structural and dynamic properties of fcc aluminium: molecular dynamics, the self-consistent ab-initio *lattice dynamics (SCAILD) and the decoupled anharmonic mode approximation (DAMA) in order to calculate vibrational eigenstates beyond the harmonic approximation typically used in lattice dynamics. The basic idea of SCAILD is to simultaneously excite phonon modes with a finite amplitude and to calculate the dynamical matrix according to the observed forces within the harmonic approximation. At given T, amplitudes – and thus also the repulsive forces – increase until self-consistency is achieved, which leads to a blue-shift of phonon modes with SCAILD (Figure 2). In contrast to harmonic lattice dynamics, DAMA takes into account the full potential energy surface along the eigenmodes in an independent particle approximation and – similar to harmonic lattice dynamics – describes the phonon interaction up to second order. From the small differences of phonon frequencies between DAMA and the harmonic approximation we infer that for stiff materials, like aluminium, vibrational frequencies can reliably be calculated in the harmonic approximation. The implementation of* $\mathbf{q}$*-DAMA and its application to aluminium shows that vibrational modes can be calculated robustly for stable-mode materials, at low computational costs. This encourages its future exploration for materials with strong anharmonicities, including materials with soft modes.*

Beyond phonon frequencies we have explored the radial distribution function and the mean square displacement in fcc aluminium. Anharmonicity is most prominent for physical quanti-

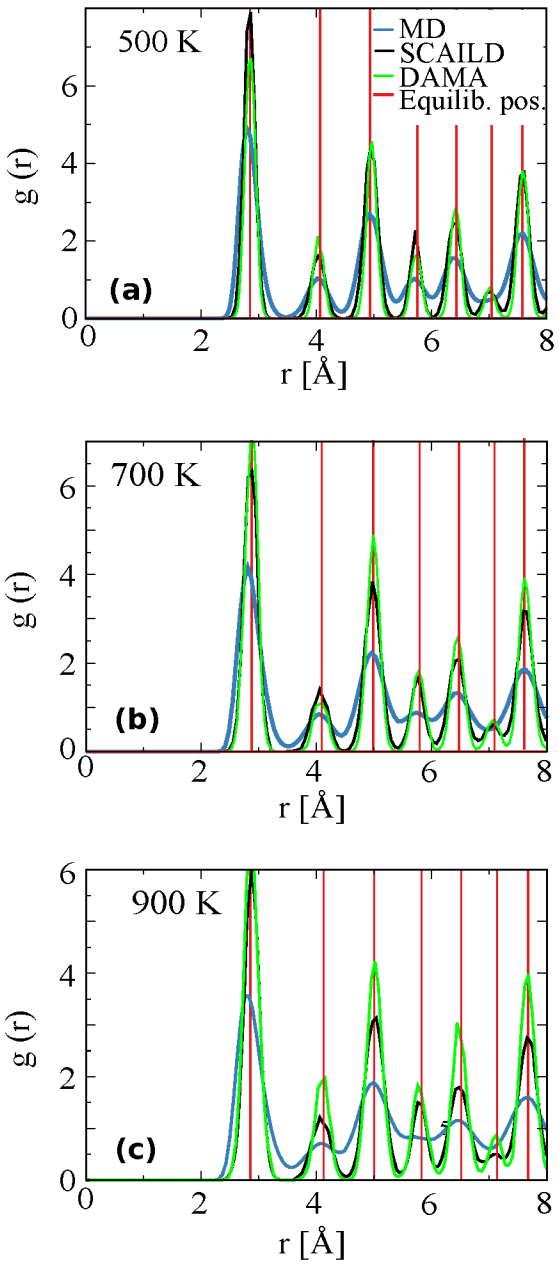

FIG. 6. Radial distribution function for the atomic distances in aluminium at 500 K (a), 700 K (b) and 900 K (c) for the equilibrium lattice (red), MD (blue), SCAILD (black) and DAMA (green) simulations.

ties that involve contributions from excited states, and DAMA describes atomic displacement better than SCAILD, based on the principle that vibrational wave functions are less extended in DAMA (Figure 3). The stronger localisation of the phonon-wave functions in DAMA yields smaller atomic displacements (Figure 5), in good agreement with experiments. As

such, the corresponding radial distribution functions calculated with DAMA (Figure 6) are expected to be accurate for aluminium and beyond. The stronger confinement of the atoms in DAMA, in turn, lifts the excitation energies with high index and reduces the vibrational contribution to the lattice heat capacity (Figure 4) compared to harmonic lattice dynamics and SCAILD.

V. ACKNOWLEDGEMENTS

We thank Empa (Empa - Swiss Federal Laboratories for Materials Science and Technology), CSCS (Swiss National Supercomputing Centre) and Leibniz Computer Centre of the Bavarian Academy of Sciences and the Humanities for computational infrastructure. The work of LW, VV and GSN was supported by the German Science Foundation (Deutsche Forschungsgemeinschaft, DFG) by grant STE1105/13-1 within the Research Unit FOR2440. We greatly appreciate helpful discussions with Vojtěch Vlček (UC Santa Barbara) and Florian Trybel (Bayerisches Geoinstitut).

[1] *L. Vocadlo and D. Alfe, Ab initio melting curve of the fcc phase of aluminum, Phys. Rev. B* ***65****, 214105 (2002).*

[2] *M. J. Tambe, N. Bonini, and N. Marzari, Bulk aluminum at high pressure: A first-principles study, Phys. Rev. B.* ***77****, 172102 (2008).*

[3] *V. Vlcek, N. de Koker, and G. Steinle-Neumann, Electrical and thermal conductivity of al liquid at high pressures and temperatures from ab initio computations, Phys. Rev. B* ***85****, 184201 (2012).*

[4] *R. Bauer, A. Schmid, P. Pavone, and D. Strauch, Electron-phonon coupling in the metallic elements al, au, na, and nb: A first-principles study, Phys. Rev. B* ***57****, 11276 (1998).*

[5] *V. Recoules and J. Crocombette, Ab initio determination of electrical and thermal conductivity of liquid aluminum, Phys. Rev. B* ***72****, 104202 (2005).*

[6] *B. J. Jesson and P. A. Madden, Ab initio determination of the melting point of aluminum by thermodynamic integration, J. Chem. Phys.* ***113****, 5924 (2000).*

[7] R. Stedman and G. Nilsson, Dispersion relations for phonons in aluminum at 80 and 300 k, Phys. Rev. **145**, 492 (1966).

[8] M. Kresch, M. Lucas, O. Delaire, J. Y. Y. Lin, and B. Fultz, Phonons in aluminum at high temperatures studied by inelastic neutron scattering, Phys. Rev. B **77**, 024301 (2008).

[9] L.-M. Peng, G. Ren, S. L. Dudarev, and M. J. Whelan, Debye–waller factors and absorptive scattering factors of elemental crystals, Acta Crystallogr., Sect. A **52**, 456 (1996).

[10] B. B. L. Witte, G. Röpke, P. Neumayer, M. French, P. Sperling, V. Recoules, S. H. Glenzer, and R. Redmer, Comment on "isochoric, isobaric, and ultrafast conductivities of aluminum, lithium, and carbon in the warm dense matter regime", Phys. Rev. E **99**, 047201 (2019).

[11] R. P. Feynman, Forces in molecules, Phys. Rev. **56**, 340 (1939).

[12] J. Neumann, Proof of the quasi-ergodic hypothesis, Proc. Natl. Acad. Sci. U.S.A. **18**, 70 (1932).

[13] H. Nagashima, S.-i. Tsuda, N. Tsuboi, M. Koshi, A. K. Hayashi, and T. Tokumasu, An analysis of the quantum effect on the thermodynamic and transport properties of cryogenic hydrogen using molecular dynamics method, J. Phys. Conf. Ser. **490**, 012160 (2014).

[14] P. Giannozzi, S. de Gironcoli, P. Pavone, and S. Baroni, Ab initio calculation of phonon dispersions in semiconductors, Phys. Rev. B **43**, 7231 (1991).

[15] D. Alfe, Phon: A program to calculate phonons using the small displacement method, Comput. Phys. Commun. **180**, 2622 (2009).

[16] F. Dorner, Z. Sukurma, C. Dellago, and G. Kresse, Melting si: Beyond density functional theory, Phys. Rev. Lett. **121**, 195701 (2018).

[17] L. Yuan and G. Steinle-Neumann, Strong sequestration of hydrogen into the earth's core during planetary differentiation, Geophys. Res. Lett. **47**, e2020GL088303 (2020).

[18] T. Tadano, Y. Gohda, and S. Tsuneyuki, Anharmonic force constants extracted from first-principles molecular dynamics: applications to heat transfer simulations, J. Phys.: Condens. Matter **26**, 225402 (2014).

[19] I. Errea, M. Calandra, and F. Mauri, Anharmonic free energies and phonon dispersions from the stochastic self-consistent harmonic approximation: Application to platinum and palladium hydrides, Phys. Rev. B **89**, 064302 (2014).

[20] P. Souvatzis, O. Eriksson, M. Katsnelson, and S. Rudin, Entropy driven stabilization of energetically unstable crystal structures explained from first principles theory, Phys. Rev. Lett.

***100**, 095901 (2008).*

*[21] D. J. Adams and D. Passerone, Insight into structural phase transitions from the decoupled anharmonic mode approximation, J. Phys. Cond. Matt. **28**, 305401 (2016).*

*[22] N. Antolin, O. D. Restrepo, and W. Windl, Fast free-energy calculations for unstable high-temperature phases, Phys. Rev. B **86**, 054119 (2012).*

*[23] A. Heiming, W. Petry, J. Trampenau, M. Alba, C. Herzig, H. R. Schober, and G. Vogl, Phonon dispersion of the bcc phase of group-iv metals. ii. bcc zirconium, a model case of dynamical precursors of martensitic transitions, Phys. Rev. B **43**, 10948 (1991).*

[24] D. R. Lide, CRC handbook of chemistry and physics*, Vol. 85 (CRC press, 2004).*

[25] T. B. Massalski, H. Okamoto, P. Subramanian, and L. Kacprzak, Binary alloy phase diagrams. vol. 3 *(ASM International, 1990) p. 1485.*

*[26] W. Petry, A. Heiming, J. Trampenau, M. Alba, C. Herzig, H. R. Schober, and G. Vogl, Phonon dispersion of the bcc phase of group-iv metals. i. bcc titanium, Phys. Rev. B **43**, 10933 (1991).*

*[27] J. Trampenau, A. Heiming, W. Petry, M. Alba, C. Herzig, W. Miekeley, and H. R. Schober, Phonon dispersion of the bcc phase of group-iv metals. iii. bcc hafnium, Phys. Rev. B **43**, 10963 (1991).*

*[28] S. Nose, A molecular dynamics method for simulations in the canonical ensemble, Mol. Phys. **52**, 255 (1984).*

[29] D. J. Adams and A. R. Oganov, Ab initio *molecular dynamics study of CaSiO_3 perovskite at* P-T *conditions of Earth's lower mantle, Phys. Rev. B **73**, 184106 (2006).*

*[30] G. Kresse and J. Furthmuller, Efficient iterative schemes for ab initio total-energy calculations using a plane-wave basis set, Phys. Rev. B **54**, 11169 (1996).*

[31] S. Baroni, A. Dal Corso, S. de Gironcoli, and P. Giannozzi, http://www.pwscf.org (2010).

*[32] J. P. Perdew, K. Burke, and M. Ernzerhof, Generalized gradient approximation made simple, Phys. Rev. Lett. **77**, 3865 (1996).*

*[33] G. Kresse and J. Hafner, Norm-conserving and ultrasoft pseudopotentials for first-row and transition-elements, J. Phys.: Condens. Matter **6**, 8245 (1994).*

*[34] A. Dal Corso, A. Pasquarello, A. Baldereschi, and R. Car, Generalized-gradient approximations to density-functional theory: A comparative study for atoms and solids, Phys. Rev. B **53**, 1180 (1996).*

[35] P. Giannozzi, S. Baroni, N. Bonini, M. Calandra, R. Car, C. Cavazzoni, D. Ceresoli, G. L. Chiarotti, M. Cococcioni, I. Dabo, A. D. Corso, S. de Gironcoli, S. Fabris, G. Fratesi, R. Gebauer, U. Gerstmann, C. Gougoussis, A. Kokalj, M. Lazzeri, L. Martin-Samos, N. Marzari, F. Mauri, R. Mazzarello, S. Paolini, A. Pasquarello, L. Paulatto, C. Sbraccia, S. Scandolo, G. Sclauzero, A. P. Seitsonen, A. Smogunov, P. Umari, and R. M. Wentzcovitch, QUANTUM ESPRESSO: a modular and open-source software project for quantum simulations of materials, J. Phys.: Condens. Matter **21**, 395502 (2009).

[36] A. J. C. Wilson, The thermal expansion of aluminium: Further experiments, Proc. Phys. Soc. London **54**, 487 (1942).

[37] S. Nenno and J. W. Kauffman, Detection and determination of equilibrium vacancy concentrations in aluminum, J. Phys. Soc. Japan **15**, 220 (1960).

[38] A. J. C. Wilson, The thermal expansion of aluminium from 0 to 650 °c, Proc. Phys. Soc. London **53**, 235 (1941).

[39] B. Grabowski, T. Hickel, and J. Neugebauer, Ab initio study of the thermodynamic properties of nonmagnetic elementary fcc metals: Exchange-correlation-related error bars and chemical trends, Phys. Rev. B **76**, 024309 (2007).

[40] R. Stedman, L. Almqvist, and G. Nilsson, Phonon-frequency distributions and heat capacities of aluminum and lead, Phys. Rev. **162**, 549 (1967).

[41] Y. Touloukian and E. Buyco, Thermophysical Properties of Matter, Vol. 4 (IFI/Plenum, New York, 1970) pp. 1–102.

[42] M. I. Katsnelson, A. Maksyutov, and A. V. Trefilov, Peculiarities of anharmonic effects in the lattice thermodynamics of fcc metals, Phys. Lett. A **295**, 50 (2002).

[43] M. Nakamura, M. Arai, Y. Inamura, T. Otomo, and S. Bennington, Effect of low-energy dynamics on anomalous vibrational amplitudes in vitreous silica, Phys. Rev. B **66**, 024203 (2002).

[44] M. Benoit, S. Ispas, and R. Jullien, Model of silica glass from combined classical and ab initio molecular-dynamics simulations, Eur. Phys. J. B **13**, 631 (2000).

[45] F. Wagle, G. Steinle-Neumann, and N. de Koker, Resistivity saturation in liquid iron–light-element alloys at conditions of planetary cores from first principles computations, Comptes Rendus Geoscience **351**, 154 (2019).

[46] C. Faber, P. Boulanger, C. Attaccalite, E. Cannuccia, I. Duchemin, T. Deutsch, and X. Blase, *Exploring approximations to the gw self-energy ionic gradients*, Phys. Rev. B **91**, 155109 (2015).

[47] G. Antonius, S. Poncé, P. Boulanger, M. Côté, and X. Gonze, *Many-body effects on the zero-point renormalization of the band structure*, Phys. Rev. Lett. **112**, 215501 (2014).

[48] M. Pozzo and D. Alfè, *Saturation of electrical resistivity of solid iron at earth's core conditions*, SpringerPlus **5**, 256 (2016).

[49] D. Alfè, M. Pozzo, and M. P. Desjarlais, *Lattice electrical resistivity of magnetic bcc iron from first-principles calculations*, Phys. Rev. B **85**, 024102 (2012).

[50] J. Xu, P. Zhang, K. Haule, J. Minar, S. Wimmer, H. Ebert, and R. E. Cohen, *Thermal conductivity and electrical resistivity of solid iron at earth's core conditions from first principles*, Phys. Rev. Lett. **121**, 096601 (2018).